This manuscript has been published in:
Wave Motion, Vol. 76 (2018), pp. 28-41.
DOI: 10.1016/j.wavemoti.2017.07.009

Second-harmonic generation in a multilayered structure with nonlinear spring-type interfaces embedded between two semi-infinite media

Yosuke Ishii[*, 1], Shiro Biwa[2], and Tadaharu Adachi[1]

[1]*Department of Mechanical Engineering, Toyohashi University of Technology, 1-1 Hibarigaoka, Tempaku-cho, Toyohashi 441-8580, Japan*

[2]*Department of Aeronautics and Astronautics, Graduate School of Engineering, Kyoto University, Katsura, Nishikyo-ku, Kyoto 615-8540, Japan*

Abstract

The acoustic second-harmonic generation behavior in a multilayered structure with nonlinear spring-type interlayer interfaces is analyzed theoretically to investigate the frequency dependence of second-harmonic amplitudes in the reflected and transmitted fields when the structure is subjected to the normal incidence of a monochromatic longitudinal wave. The multilayered structure consists of identical linear elastic layers and is embedded between two identical linear elastic semi-infinite media. The layers are bonded to each other by spring-type interfaces possessing identical linear stiffness but different quadratic nonlinear parameters. By combining a perturbation analysis with the transfer-matrix method, analytical expressions are derived for the second-harmonic amplitudes of the reflected and transmitted waves. The second-harmonic amplitudes due to a single nonlinear interface are shown to vary remarkably with the fundamental frequency, reflecting the pass and stop band characteristics of the Bloch wave in the corresponding infinitely extended layered structure. By calculating the spatial distribution of second-harmonic amplitude inside the multilayered structure, the influence of the position of the nonlinear interface as well as the number of layers on the frequency dependence of second-harmonic amplitudes of the reflected and transmitted waves is elucidated. When all interlayer interfaces possess the identical nonlinearity, the second-harmonic amplitudes on both sides of the structure are shown to increase monotonically with the number of layers in the frequency ranges where both fundamental and double frequencies are within the pass bands of Bloch wave. The influence of two non-dimensional parameters, i.e., the relative linear compliance of the interlayer interfaces and the acoustic impedance ratio between the layer and the surrounding semi-infinite medium, on the second-harmonic amplitudes is elucidated.

Key Words: Multilayered structure; Nonlinear acoustics; Harmonic generation; Perturbation analysis; Spring-type interface; Transfer-matrix method

* Corresponding author: Yosuke Ishii, E-mail: ishii@me.tut.ac.jp

1. Introduction

Multilayered structures are found in various technological products and in nature such as advanced fiber-reinforced composite laminates in aerospace engineering, glued laminated timbers called glulam in architectural engineering, laminated rubber bearings for the seismic isolation in civil engineering, and stratified rocks in the Earth's crust. In such structures, many different types of imperfections can occur at the interfaces between neighboring layers: thin interphase layers, kissing bonds, closed cracks and delaminations, fractures, and so on. Understanding the influence of these imperfections on the wave propagation characteristics is essential from the viewpoints of the ultrasonic nondestructive testing in engineering practice, the seismic survey in oil and gas exploration, and the risk assessment of earthquake.

Foregoing studies have revealed that the elastic wave interaction with such imperfect interfaces can be analyzed by modeling them as spring-type interfaces [1]-[7]: the stresses are continuous while the displacements are allowed to be discontinuous across the interface, and the resulting jumps of displacements are related to the stresses by the proportional constants called interfacial stiffnesses. Spring-type interface models have been utilized extensively to characterize a contacting interface between rough surfaces of solid bodies [8]-[13], a partially closed crack [14], [15], concentration of microcracks [16]-[18], a fracture in rock mass [19]-[23], adhesion at double interfaces between an adhesive layer and two adherents [24]-[28], multiple interlayer thin resin-rich zones of polymer-based composite laminates [29]-[33], and multiple rock joints [34], [35].

On the other hand, when these imperfect interfaces are insonified by waves with sufficiently high amplitude, they can be a source of nonlinear acoustic phenomena. Among others, the higher-harmonic generation has been studied theoretically as well as experimentally in the field of ultrasonic nondestructive testing for more sensitive characterization of the interface quality than the conventional techniques based on the linear wave propagation characteristics [36]-[41]. According to the foregoing studies [42]-[48], the generation behavior of the second- or higher-order harmonics at a

solid-solid contacting interface can be reasonably described by the nonlinear spring-type interface model. Using this model, Yan et al. [49], [50] studied the second-harmonic generation at a kissing bond on one of the double interfaces between an adhesive layer and two aluminum blocks. The wave interaction with double nonlinear spring-type interfaces was also analyzed by Junca and Lombard [51]. For the more general case of multiple interfaces, Biwa and Ishii [52] analyzed the propagation characteristics of the Bloch wave in infinitely layered structures with spring-type interlayer interfaces possessing a weak quadratic nonlinearity. They elucidated the frequency dependence of the second-harmonic generation in the structures based on their pass and stop band characteristics. For finite layered structures with nonlinear spring-type interlayer interfaces, Ishii and Biwa [53] showed some preliminary numerical results of the frequency dependence of second-harmonic amplitudes of the reflected and transmitted waves by combining a perturbation approach with the transfer-matrix method [54], [55], while they left out the details of the corresponding mathematical expressions. Better understanding of this issue is important from fundamental and practical points of view to characterize the imperfect interlayer interfaces of multilayered structures by using nonlinear acoustic methods.

In this paper, the formulations omitted in Ref. [53] is fully described and the second-harmonic generation behavior in multilayered structures is analyzed in a more precise manner. Namely, the present analysis deals with the second-harmonic generation in a finite layered structure with nonlinear spring-type interlayer interfaces when it is subjected to the normal incidence of a monochromatic longitudinal wave, and elucidate the frequency dependence of second-harmonic amplitudes in the reflected and transmitted fields. Following the perturbation analysis for a weak quadratic nonlinearity of interfaces carried out in Ref. [52], the governing equations for the propagation of fundamental wave and its second-harmonic component in the structure embedded between two linear elastic semi-infinite media are presented in the frequency domain in Section 2. The solution to the fundamental wave propagation, i.e., the amplitude reflection and transmission coefficients as well as the displacement

jumps at the interlayer interfaces, is obtained using the transfer-matrix method in Section 3. The explicit expressions for the second-harmonic amplitudes of the reflected and transmitted waves are derived in Section 4. The resulting frequency dependence of the second-harmonic amplitude due to a single as well as multiple nonlinear interlayer interfaces is discussed in Section 5.

2. Formulation

The one-dimensional longitudinal wave propagation in the layering direction of a multilayered structure is considered. The position is denoted by x. The structure consists of N identical linear elastic layers (density ρ, wave velocity c, and thickness h) and is embedded between two identical linear elastic semi-infinite media (density ρ_0 and wave velocity c_0) with the perfect bonding at $x = X_0$ and $x = X_N$ as shown in Fig. 1. Using the displacement $u(x,t)$ where t is the time, the stress $\sigma(x,t)$ is given by

$$\sigma(x,t) = \rho c^2 \frac{\partial u}{\partial x}(x,t), \tag{1}$$

in the layer and

$$\sigma(x,t) = \rho_0 c_0^2 \frac{\partial u}{\partial x}(x,t), \tag{2}$$

in the semi-infinite medium.

The layers are bonded to each other by spring-type interfaces at $x = X_m = X_0 + mh$ (m = 1, 2, 3…, N-1), where the stress is continuous while the discontinuity is allowed in the displacement. When the spring-type interfaces possess weak quadratic nonlinearity [43], the boundary conditions for the mth interface are given by [52], [53]

$$\sigma(X_{m+},t) = \sigma(X_{m-},t) = K_{\mathrm{S}}[1 - \beta_m y_m(t)]y_m(t), \tag{3}$$

where the subscripts "+" and "–" denote the limit of a field variable when x approaches the corresponding coordinate from the positive and negative sides, respectively. In Eq. (3), K_S is the linear interfacial stiffness, which is assumed to be the same for all interfaces, β_m is a positive parameter representing the nonlinearity of the mth interface, and $y_m(t)$ is the gap distance at $x = X_m$ defined by

$$y_m(t) \equiv u(X_{m+}, t) - u(X_{m-}, t). \tag{4}$$

The present study analyzes the amplitudes of the nonlinearly generated second-harmonic component in the reflected and transmitted waves for $x < X_0$ and $x > X_N$, respectively, when a monochromatic longitudinal wave with angular frequency ω_0 and amplitude A_I impinges perpendicularly on the multilayered structure from $x < X_0$. Assuming that $\mathrm{Max}_m[\beta_m]A_I$ is sufficiently small, and that the time dependence term is given by exp(-iωt) where $i^2 = -1$ and ω is the angular frequency, the governing equations and the boundary conditions for the fundamental wave ($\omega = \omega_0$) and its second-harmonic component ($\omega = 2\omega_0$) are written by performing the perturbation analysis [52] as

For $\omega = \omega_0$;

$$\frac{\mathrm{d}^2 U_1}{\mathrm{d}x^2} + \frac{\omega_0^2}{c_0^2} U_1 = 0, \qquad x < X_0 \text{ and } x > X_N, \tag{5}$$

$$\frac{\mathrm{d}^2 U_1}{\mathrm{d}x^2} + \frac{\omega_0^2}{c^2} U_1 = 0, \qquad X_{p-1} < x < X_p, \qquad p = 1,2,\dots,N, \tag{6}$$

$$\rho c^2 \frac{\mathrm{d}U_1}{\mathrm{d}x}(X_{m+}) = \rho c^2 \frac{\mathrm{d}U_1}{\mathrm{d}x}(X_{m-}) = K_S Y_{1m}, \qquad m = 1,2,\dots,N-1, \tag{7}$$

$$U_1(X_{q+}) = U_1(X_{q-}), \qquad q = 0, N, \tag{8}$$

$$\rho c^2 \frac{\mathrm{d}U_1}{\mathrm{d}x}(X_{0+}) = \rho_0 c_0^2 \frac{\mathrm{d}U_1}{\mathrm{d}x}(X_{0-}), \qquad \rho_0 c_0^2 \frac{\mathrm{d}U_1}{\mathrm{d}x}(X_{N+}) = \rho c^2 \frac{\mathrm{d}U_1}{\mathrm{d}x}(X_{N-}), \tag{9}$$

For $\omega = 2\omega_0$;

$$\frac{\mathrm{d}^2 U_2}{\mathrm{d}x^2} + \frac{(2\omega_0)^2}{c_0^2} U_2 = 0, \qquad x < X_0 \text{ and } x > X_N, \tag{10}$$

$$\frac{\mathrm{d}^2 U_2}{\mathrm{d}x^2} + \frac{(2\omega_0)^2}{c^2} U_2 = 0, \qquad X_{p-1} < x < X_p, \qquad p = 1,2,\dots,N, \tag{11}$$

$$\rho c^2 \frac{\mathrm{d}U_2}{\mathrm{d}x}(X_{m+}) = \rho c^2 \frac{\mathrm{d}U_2}{\mathrm{d}x}(X_{m-}) = K_\mathrm{S} Y_{2m} - \frac{1}{2}\beta_m K_\mathrm{S} Y_{1m}^2, \qquad m = 1,2,\dots,N-1, \tag{12}$$

$$U_2(X_{q+}) = U_2(X_{q-}), \qquad q = 0, N, \tag{13}$$

$$\rho c^2 \frac{\mathrm{d}U_2}{\mathrm{d}x}(X_{0+}) = \rho_0 c_0^2 \frac{\mathrm{d}U_2}{\mathrm{d}x}(X_{0-}), \qquad \rho_0 c_0^2 \frac{\mathrm{d}U_2}{\mathrm{d}x}(X_{N+}) = \rho c^2 \frac{\mathrm{d}U_2}{\mathrm{d}x}(X_{N-}), \tag{14}$$

where U_1 and U_2 (Y_{1m} and Y_{2m}) are the complex-valued time-harmonic displacements (gap distances of interlayer interfaces) of the fundamental wave and its second-harmonic component, respectively.

3. Analysis of fundamental wave propagation

The fundamental wave propagation governed by Eqs. (5)-(9) is first analyzed here by using the transfer-matrix method [54], [55] to obtain the amplitude reflection and transmission coefficients of the fundamental wave as well as the gap distances of the interlayer interfaces Y_{1m} which are required to calculate the second-harmonic generation at the nonlinear interfaces in Eq. (12).

3.1. Calculation of the amplitude reflection and transmission coefficients

As a solution to Eqs. (5) and (6), the forward- and backward-propagating waves denoted by $U_{1\mathrm{F}}(x)$ and $U_{1\mathrm{B}}(x)$ are considered, respectively. The displacement vector is then defined as $\mathbf{U}_1(x) \equiv (U_{1\mathrm{F}}(x), U_{1\mathrm{B}}(x))^\mathrm{T}$, where the superscript "T" denotes the transpose.

The displacement vectors on the left ($x = X_{0-}$) and the right ($x = X_{N+}$) sides of the multilayered structure are written as

$$\mathbf{U}_1(X_{0-}) = \begin{pmatrix} A_\mathrm{I} \exp(\mathrm{i}\Omega \widehat{X_0}) \\ R_1(\Omega) A_\mathrm{I} \exp(-\mathrm{i}\Omega \widehat{X_0}) \end{pmatrix}, \tag{15}$$

$$\mathbf{U}_1(X_{N+}) = \begin{pmatrix} T_1(\Omega) A_\mathrm{I} \exp(\mathrm{i}\Omega \widehat{X_N}) \\ 0 \end{pmatrix}, \tag{16}$$

where $\Omega \equiv \omega_0 h/c$ and $\widehat{X_q} \equiv c X_q/(c_0 h)$ (q = 0, N) represent the normalized angular frequency and

the normalized positions of the boundaries between the structure and the surrounding semi-infinite media, respectively. In Eqs. (15) and (16), $R_1(\Omega)$ and $T_1(\Omega)$ denote the complex-valued amplitude reflection and transmission coefficients, respectively. These are calculated by applying the transfer-matrix method [54], [55] to Eqs. (5)-(9) as,

$$R_1(\Omega) = -\frac{L_{21}(\Omega)}{L_{22}(\Omega)}\exp\left(2\mathrm{i}\Omega\widehat{X_0}\right), \tag{17}$$

$$T_1(\Omega) = \frac{L_{11}(\Omega)L_{22}(\Omega) - L_{12}(\Omega)L_{21}(\Omega)}{L_{22}(\Omega)}\exp\left[-\mathrm{i}\Omega\left(\widehat{X_N} - \widehat{X_0}\right)\right]. \tag{18}$$

In the above expressions, $L_{IJ}(\Omega)$ (I, J = 1, 2) are the elements of the global transfer matrix given by [29]-[32]

$$\begin{aligned}\mathbf{L}(\Omega) &= \begin{bmatrix} L_{11}(\Omega) & L_{12}(\Omega) \\ L_{21}(\Omega) & L_{22}(\Omega) \end{bmatrix} \\ &= \mathbf{T}_{\mathrm{LS}}\mathbf{P}(\Omega)[\mathbf{S}(\Omega)\mathbf{P}(\Omega)]^{N-1}\mathbf{T}_{\mathrm{SL}} \\ &= \mathbf{T}_{\mathrm{LS}}\mathbf{S}(\Omega)^{-1}\mathbf{H}(\Omega)^{N}\mathbf{T}_{\mathrm{SL}},\end{aligned} \tag{19}$$

where

$$\mathbf{S}(\Omega) = \begin{bmatrix} 1 + \mathrm{i}\Lambda\Omega & -\mathrm{i}\Lambda\Omega \\ \mathrm{i}\Lambda\Omega & 1 - \mathrm{i}\Lambda\Omega \end{bmatrix}, \tag{20}$$

$$\mathbf{P}(\Omega) = \begin{bmatrix} \exp(\mathrm{i}\Omega) & 0 \\ 0 & \exp(-\mathrm{i}\Omega) \end{bmatrix}, \tag{21}$$

$$\mathbf{H}(\Omega) \equiv \mathbf{S}(\Omega)\mathbf{P}(\Omega) = \begin{bmatrix} (1 + \mathrm{i}\Lambda\Omega)\exp(\mathrm{i}\Omega) & -\mathrm{i}\Lambda\Omega\exp(-\mathrm{i}\Omega) \\ \mathrm{i}\Lambda\Omega\exp(\mathrm{i}\Omega) & (1 - \mathrm{i}\Lambda\Omega)\exp(-\mathrm{i}\Omega) \end{bmatrix}, \tag{22}$$

$$\mathbf{T}_{\mathrm{SL}} = \frac{1}{2\zeta}\begin{bmatrix} \zeta + 1 & \zeta - 1 \\ \zeta - 1 & \zeta + 1 \end{bmatrix}, \tag{23}$$

$$\mathbf{T}_{\mathrm{LS}} = \frac{1}{2}\begin{bmatrix} 1 + \zeta & 1 - \zeta \\ 1 - \zeta & 1 + \zeta \end{bmatrix}, \tag{24}$$

where $\mathbf{S}(\Omega)$ is the scattering matrix of the interlayer interface, $\mathbf{P}(\Omega)$ is the propagator matrix in the layer, and $\mathbf{T}_{\mathrm{SL}}$ and $\mathbf{T}_{\mathrm{LS}}$ are the scattering matrices of the perfectly bonded interfaces at $x = X_0$ and x

$= X_N$, respectively. In the above expressions, the non-dimensional parameters

$$\Lambda \equiv \frac{\rho c^2}{2K_S h}, \tag{25}$$

$$\zeta \equiv \frac{\rho c}{\rho_0 c_0}, \tag{26}$$

represent the relative linear compliance of the interlayer interfaces and the acoustic impedance ratio between the layer and the semi-infinite medium, respectively.

By introducing the Bloch wavenumber $K(\Omega)$ for the infinitely extended layered structure whose unit-cell consists of one layer and one linearized spring-type interface given by [31], [52]

$$\exp[\mathrm{i}K(\Omega)h] = G(\Omega) \pm \mathrm{i}\sqrt{1 - G(\Omega)^2}, \tag{27}$$

$$G(\Omega) \equiv \cos\Omega - \Lambda\Omega\sin\Omega, \tag{28}$$

$\mathbf{H}(\Omega)^N$ in Eq. (19) can be written as

$$\mathbf{H}(\Omega)^N = \begin{cases} \dfrac{\sin[N\alpha_1(\Omega)h]}{\sin[\alpha_1(\Omega)h]}\mathbf{H}(\Omega) - \dfrac{\sin[(N-1)\alpha_1(\Omega)h]}{\sin[\alpha_1(\Omega)h]}\mathbf{I}, & \alpha_1(\Omega) \neq n\pi/h, \alpha_2(\Omega) = 0, \quad (29a) \\ (-1)^{n(N+1)}\dfrac{\sinh[N\alpha_2(\Omega)h]}{\sinh[\alpha_2(\Omega)h]}\mathbf{H}(\Omega) - (-1)^{nN}\dfrac{\sinh[(N-1)\alpha_2(\Omega)h]}{\sinh[\alpha_2(\Omega)h]}\mathbf{I}, & \alpha_1(\Omega) = n\pi/h, \alpha_2(\Omega) \neq 0, \quad (29b) \\ (-1)^{n(N+1)}N\mathbf{H}(\Omega) - (-1)^{nN}(N-1)\mathbf{I}, & \alpha_1(\Omega) = n\pi/h, \alpha_2(\Omega) = 0, \quad (29c) \end{cases}$$

where $\mathbf{I}$ is the 2×2 identity matrix, n is an integer, and $\alpha_1(\Omega)$ and $\alpha_2(\Omega)$ are the real and imaginary parts of the Bloch wavenumber, respectively, i.e., $K(\Omega) \equiv \alpha_1(\Omega) + \mathrm{i}\,\alpha_2(\Omega)$. For the derivation of Eq. (29a), refer to Ref. [56]. Equation (29b) can be obtained from Eq. (29a) with the relation $\sin[n\pi + \mathrm{i}\alpha_2(\Omega)] = \mathrm{i}(-1)^n \sinh[\alpha_2(\Omega)]$, and then Eq. (29c) is given by applying L'Hôpital's rule to Eq. (29b). Equations (29a)-(29c) correspond to the pass bands, stop bands, and boundaries between the pass and stop bands of the infinitely periodic structure, respectively.

From Eqs. (19)-(24) and (29) with the property that $\det[\mathbf{L}(\Omega)] = 1$, Eqs. (17) and (18) can be rewritten explicitly as,

$$R_1(\Omega) = \frac{D_3}{D_1 + \mathrm{i}D_2} \exp\left(2\mathrm{i}\Omega\widehat{X_0}\right), \tag{30}$$

$$T_1(\Omega) = \frac{\mathrm{i}D_4}{D_1 + \mathrm{i}D_2} \exp\left[-\mathrm{i}\Omega\left(\widehat{X_N} - \widehat{X_0}\right)\right], \tag{31}$$

where D_k (k = 1, 2, 3, 4) are real numbers given by

$$D_1 = 2\Lambda\Omega \sin[(N-1)\alpha_1(\Omega)h] + (\zeta^2 + 1) \sin[N\alpha_1(\Omega)h] \sin\Omega, \tag{32a}$$

$$D_2 = 2\zeta\{\sin[N\alpha_1(\Omega)h] \cos\Omega - \sin[(N-1)\alpha_1(\Omega)h]\}, \tag{32b}$$

$$D_3 = 2\Lambda\Omega \sin[(N-1)\alpha_1(\Omega)h] - (\zeta^2 - 1) \sin[N\alpha_1(\Omega)h] \sin\Omega, \tag{32c}$$

$$D_4 = 2\zeta \sin[\alpha_1(\Omega)h], \tag{32d}$$

when $\alpha_1(\Omega) \neq n\pi/h$ and $\alpha_2(\Omega) = 0$,

$$D_1 = 2\Lambda\Omega \sinh[(N-1)\alpha_2(\Omega)h] + (-1)^n(\zeta^2 + 1) \sinh[N\alpha_2(\Omega)h] \sin\Omega, \tag{33a}$$

$$D_2 = 2\zeta\{(-1)^n \sinh[N\alpha_2(\Omega)h] \cos\Omega - \sinh[(N-1)\alpha_2(\Omega)h]\}, \tag{33b}$$

$$D_3 = 2\Lambda\Omega \sinh[(N-1)\alpha_2(\Omega)h] - (-1)^n(\zeta^2 - 1) \sinh[N\alpha_2(\Omega)h] \sin\Omega, \tag{33c}$$

$$D_4 = 2(-1)^{nN}\zeta \sinh[\alpha_2(\Omega)h], \tag{33d}$$

when $\alpha_1(\Omega) = n\pi/h$ and $\alpha_2(\Omega) \neq 0$, and

$$D_1 = 2\Lambda\Omega(N-1) + (-1)^n(\zeta^2 + 1)N \sin\Omega, \tag{34a}$$

$$D_2 = 2\zeta[1 + (-1)^n N\Lambda\Omega \sin\Omega], \tag{34b}$$

$$D_3 = 2\Lambda\Omega(N-1) - (-1)^n(\zeta^2 - 1)N \sin\Omega, \tag{34c}$$

$$D_4 = 2(-1)^{nN}\zeta, \tag{34d}$$

when $\alpha_1(\Omega) = n\pi/h$ and $\alpha_2(\Omega) = 0$.

3.2. Calculation of the gap distance at the interlayer interfaces

The gap distance at the mth interlayer interface (m = 1, 2, …, N-1) due to the fundamental wave

propagation can be written by using $\mathbf{U}_1(X_{m+}) = \mathbf{S}(\Omega)\mathbf{U}_1(X_{m-})$, $\mathbf{S}(\Omega)^{-1} = \mathbf{S}(-\Omega)$, $\mathbf{P}(\Omega)^{-1} = \mathbf{P}(-\Omega)$, and $\mathbf{T}_{\mathrm{LS}}^{-1} = \mathbf{T}_{\mathrm{SL}}$ as

$$\begin{aligned} Y_{1m}(\Omega) &= U_{1\mathrm{F}}(X_{m+}) + U_{1\mathrm{B}}(X_{m+}) - U_{1\mathrm{F}}(X_{m-}) - U_{1\mathrm{B}}(X_{m-}) \\ &= 2\mathrm{i}\Lambda\Omega\mathbf{g}\,\mathbf{U}_1(X_{m-}) \\ &= 2\mathrm{i}\Lambda\Omega\mathbf{g}\,[\mathbf{S}(\Omega)^{-1}\mathbf{P}(\Omega)^{-1}]^{N-m}\mathbf{T}_{\mathrm{LS}}^{-1}\mathbf{U}_1(X_{N+}) \\ &= 2\mathrm{i}\Lambda\Omega\mathbf{g}\,\mathbf{H}(-\Omega)^{N-m}\mathbf{T}_{\mathrm{SL}}\mathbf{U}_1(X_{N+}), \end{aligned} \tag{35}$$

where $\mathbf{g} = (1, -1)$. Using Eqs. (16), (22), (23), and (29) with the so-obtained amplitude transmission coefficient from Eq. (31), the above equation is reduced to

$$Y_{1m}(\Omega) = \frac{2\mathrm{i}\Lambda\Omega A_{\mathrm{I}}}{\zeta} T_1(\Omega)\exp\left(\mathrm{i}\Omega\widehat{X_N}\right) E_{N-m}(\Omega), \tag{36}$$

where

$$E_m(\Omega) = F_{m1}(\Omega) + \mathrm{i}F_{m2}(\Omega), \tag{37}$$

and $F_{m1}(\Omega)$ and $F_{m2}(\Omega)$ are real functions defined by

$$F_{m1}(\Omega) \equiv \begin{cases} \dfrac{\sin[m\alpha_1(\Omega)h]\cos\Omega - \sin[(m-1)\alpha_1(\Omega)h]}{\sin[\alpha_1(\Omega)h]}, & \alpha_1(\Omega) \neq n\pi/h, \alpha_2(\Omega) = 0, \quad (38a) \\ \dfrac{(-1)^n \sinh[m\alpha_2(\Omega)h]\cos\Omega - \sinh[(m-1)\alpha_2(\Omega)h]}{(-1)^{nm}\sinh[\alpha_2(\Omega)h]}, & \alpha_1(\Omega) = n\pi/h, \alpha_2(\Omega) \neq 0, \quad (38b) \\ (-1)^{nm}[1 + (-1)^n m\Lambda\Omega\sin\Omega], & \alpha_1(\Omega) = n\pi/h, \alpha_2(\Omega) = 0, \quad (38c) \end{cases}$$

$$F_{m2}(\Omega) \equiv \begin{cases} \dfrac{-\zeta\sin[m\alpha_1(\Omega)h]\sin\Omega}{\sin[\alpha_1(\Omega)h]}, & \alpha_1(\Omega) \neq n\pi/h, \alpha_2(\Omega) = 0, \quad (39a) \\ \dfrac{(-1)^{n(m+1)+1}\zeta\sinh[m\alpha_2(\Omega)h]\sin\Omega}{\sinh[\alpha_2(\Omega)h]}, & \alpha_1(\Omega) = n\pi/h, \alpha_2(\Omega) \neq 0, \quad (39b) \\ (-1)^{n(m+1)+1}m\zeta\sin\Omega, & \alpha_1(\Omega) = n\pi/h, \alpha_2(\Omega) = 0. \quad (39c) \end{cases}$$

4. Calculation of the second-harmonic amplitudes of the reflected and transmitted waves

4.1. Transfer matrix formulation

As in the case of the fundamental wave propagation in Section 3, the displacement components of the forward- and backward-propagating second-harmonics which satisfy Eqs. (10) and (11) are denoted by $U_{2\mathrm{F}}(x)$ and $U_{2\mathrm{B}}(x)$, respectively, and the vector with these elements by $\mathbf{U}_2(x) \equiv (U_{2\mathrm{F}}(x), U_{2\mathrm{B}}(x))^{\mathrm{T}}$.

Using Eq. (12) with the fundamental component of interfacial gap opening given in Eq. (36), the second-harmonic displacements on both sides of the mth interlayer interface (m = 1, 2, …, N–1) are related by [52]

$$\mathbf{U}_2(X_{m+}) = \mathbf{S}(2\Omega)\mathbf{U}_2(X_{m-}) + \frac{\beta_m Y_{1m}(\Omega)^2}{4}\mathbf{e}, \tag{40}$$

where $\mathbf{e} = (1,\ 1)^{\mathrm{T}}$. In addition, the displacements at $x = X_{(p\text{-}1)+}$ and $x = X_{p-}$ (p = 1, 2, …, N) are connected as

$$\mathbf{U}_2(X_{p-}) = \mathbf{P}(2\Omega)\mathbf{U}_2(X_{(p-1)+}). \tag{41}$$

Furthermore, the perfect bonding conditions for the interfaces between the multilayered structure and the semi-infinite media in Eqs. (13) and (14) give

$$\mathbf{U}_2(X_{0+}) = \mathbf{T}_{\mathrm{SL}}\mathbf{U}_2(X_{0-}), \tag{42}$$

$$\mathbf{U}_2(X_{N+}) = \mathbf{T}_{\mathrm{LS}}\mathbf{U}_2(X_{N-}). \tag{43}$$

4.2. Multilayered structure with a single nonlinear interface

Let us consider here the situation where only the interlayer interface located at $x = X_s$ ($1 \le s \le N - 1$) possesses the non-zero nonlinearity, i.e., $\beta_m > 0$ when $m = s$ and $\beta_m = 0$ when $1 \le m \le s - 1$ or $s + 1 \le m \le N - 1$. Using Eqs. (40)-(43), the second-harmonic components at the right and left of the

structure are related by

$$\mathbf{U}_2(X_{N+}) = \mathbf{L}(2\Omega)\mathbf{U}_2(X_{0-}) + \mathbf{b}_s(\Omega), \tag{44}$$

where

$$\mathbf{b}_s(\Omega) \equiv \begin{pmatrix} b_{s1}(\Omega) \\ b_{s2}(\Omega) \end{pmatrix} = \frac{1}{4}\beta_s Y_{1s}(\Omega)^2 \mathbf{T}_{\mathrm{LS}}\mathbf{S}(2\Omega)^{-1}\mathbf{H}(2\Omega)^{N-s}\mathbf{e}. \tag{45}$$

On the other hand, Eqs. (44) and (45) can be also written as

$$\mathbf{U}_2(X_{0-}) = \mathbf{L}(2\Omega)^{-1}\mathbf{U}_2(X_{N+}) - \mathbf{c}_s(\Omega), \tag{46}$$

where

$$\mathbf{c}_s(\Omega) \equiv \begin{pmatrix} c_{s1}(\Omega) \\ c_{s2}(\Omega) \end{pmatrix} = \frac{1}{4}\beta_s Y_{1s}(\Omega)^2 \mathbf{T}_{\mathrm{LS}}\mathbf{H}(2\Omega)^{-s}\mathbf{e}. \tag{47}$$

From the physical reasoning that the generated second-harmonic component should propagate away from the multilayered structure, its displacement vectors at $x = X_{0-}$ and $x = X_{N+}$ become

$$\mathbf{U}_2(X_{0-}) = \begin{pmatrix} 0 \\ A_{\mathrm{R2}} \exp\left(-2\mathrm{i}\Omega\widehat{X_0}\right) \end{pmatrix}, \tag{48}$$

$$\mathbf{U}_2(X_{N+}) = \begin{pmatrix} A_{\mathrm{T2}} \exp\left(2\mathrm{i}\Omega\widehat{X_N}\right) \\ 0 \end{pmatrix}, \tag{49}$$

where A_{R2} and A_{T2} denote the second-harmonic amplitudes of the reflected and transmitted waves, respectively. These are given by substituting Eqs. (48) and (49) into Eqs. (44) and (46), and carrying out the straightforward calculation as

$$\begin{aligned} A_{\mathrm{R2}} &= -\frac{b_{s2}(\Omega)}{L_{22}(2\Omega)} \exp\left(2\mathrm{i}\Omega\widehat{X_0}\right) \\ &= -\frac{1}{4}T_1(2\Omega)\beta_s Y_{1s}(\Omega)^2 E_{N-s}(2\Omega) \exp\left(2\mathrm{i}\Omega\widehat{X_N}\right), \end{aligned} \tag{50}$$

$$A_{\mathrm{T2}} = \frac{c_{s1}(\Omega)}{L_{22}(2\Omega)} \exp\left(-2\mathrm{i}\Omega\widehat{X_N}\right)$$
$$= \frac{1}{4} T_1(2\Omega)\beta_s Y_{1s}(\Omega)^2 E_s(2\Omega) \exp\left(-2\mathrm{i}\Omega\widehat{X_0}\right). \tag{51}$$

Equations (50) and (51) indicate that different factors influence the second-harmonic amplitudes of the reflected and transmitted waves. First, the second-harmonic generation at the *s*th nonlinear interface is governed by the nonlinearity parameter β_s and the interfacial gap opening $Y_{1s}(\Omega)$. After being generated, the second-harmonic propagates in the multilayered structure with linearized interlayer interfaces. Its propagation efficiency is governed by the transmission coefficient at the double frequency $T_1(2\Omega)$, with the compensation for the position of the nonlinear interface in the structure $E_{N-s}(2\Omega)$ and $E_s(2\Omega)$ for the reflected and transmitted waves, respectively.

4.3. Multilayered structure with multiple nonlinear interfaces

Since the governing equations for the second harmonics in Eqs. (10)–(14) are linear, the second-harmonic amplitudes on both sides of the multilayered structure in the more general case of multiple nonlinear interfaces at $x = X_m$ (m = 1, 2, …, N–1) are now given by superposing the solution of the above single nonlinear interface problem in Eqs. (50) and (51) for different s as

$$A_{\mathrm{R2}} = -\frac{1}{4} T_1(2\Omega) \exp\left(2\mathrm{i}\Omega\widehat{X_N}\right) \sum_{m=1}^{N-1} \beta_m Y_{1m}(\Omega)^2 E_{N-m}(2\Omega), \tag{52}$$

$$A_{\mathrm{T2}} = \frac{1}{4} T_1(2\Omega) \exp\left(-2\mathrm{i}\Omega\widehat{X_0}\right) \sum_{m=1}^{N-1} \beta_m Y_{1m}(\Omega)^2 E_m(2\Omega). \tag{53}$$

5. Results and discussions

5.1. Factors governing the second-harmonic amplitudes

It has been shown in Section 4 that the second-harmonic amplitudes of the reflected and transmitted waves are governed by several factors. As an example, these factors are depicted as functions of the normalized angular frequency in Fig. 2 when $N = 4$, $\Lambda = 0.2$, and $\zeta = 3$.

As mentioned earlier, the second-harmonic generation at the sth nonlinear interface is influenced by the interfacial gap opening $|Y_{1s}(\Omega)|$ shown in Fig. 2(a). This quantity depends on, from Eq. (36), the amplitude transmission coefficient of the fundamental wave $|T_1(\Omega)|$ shown in Fig. 2(b) as well as the distance from the sth interface to the right end of the structure which is given by the factor $|E_{N-s}(\Omega)|$ shown in Fig. 2(c), both of which are related to the Bloch wavenumber of the corresponding infinitely extended layered structure at the fundamental frequency $\alpha_1(\Omega)$ and $\alpha_2(\Omega)$ shown in Fig. 2(d). It is noted that the dispersion relation is depicted only for the forward-propagating Bloch wave in Fig. 2(d). From Eqs. (38c) and (39c), $|E_s(\Omega)|$ in Fig. 2(c) becomes unity regardless of s when $\Omega = n\pi$. Namely, the gap opening is the same for all interlayer interfaces at the beginning of each pass band of the Bloch wave as can be seen in Fig. 2(a). In addition, when the frequency lies in the stop bands of Bloch wave, i.e., $\alpha_2(\Omega) > 0$, $|E_s(\Omega)|$ becomes relatively large and its peaks exhibit monotonic growth with s due to the hyperbolic nature in Eqs. (38b) and (39b). The resulting gap opening in Fig. 2(a), however, becomes relatively small in these frequency ranges since $|T_1(\Omega)|$ drops to low levels therein in Fig. 2(b).

The second-harmonic component generated at the sth interface is then influenced by the layered structure before being observed outside the structure as the reflected or transmitted wave. This effect is represented by the amplitude transmission coefficient at the double frequency $|T_1(2\Omega)|$ shown in Fig. 2(b) and the factor $|E_s(2\Omega)|$ shown in Fig. 2(e), both of which depend on the propagation behavior of Bloch wave at the double frequency $\alpha_1(2\Omega)$ and $\alpha_2(2\Omega)$ shown in Fig. 2(d).

5.2. Second-harmonic generation by a single nonlinear interface

5.2.1. Frequency dependence of the second-harmonic amplitudes of the reflected and transmitted waves

When the interlayer interface located at $x = X_s$ solely possesses the non-zero nonlinearity of $\beta_s = \beta$ where β is a positive constant, the second-harmonic amplitudes of the reflected and transmitted waves are calculated by Eqs. (50) and (51) for three cases where s = 1, N/2, and N-1. The results for different N with fixed Λ = 0.2 and ζ = 3 are shown as functions of the normalized fundamental frequency in Fig. 3(a) and 3(b) for N = 4, in Fig. 3(c) and 3(d) for N = 10, and in Fig. 3(e) and 3(f) for N = 20.

In Fig. 3, the second-harmonic amplitudes are significantly influenced not only by the frequency but also by the number of layers as well as the position of the nonlinear interface. There exist some frequency ranges in which the second-harmonic amplitude falls to vanishingly low levels, and such regions become clearer as the number of layers increases. These frequency ranges are formed at around Ω/π = 0.9 and Ω/π = 1.8 in a similar manner irrespective of the location of the nonlinear interface, and agree well with those in the case of infinitely layered structure in Ref. [52]. On the other hand, the second-harmonic amplitudes at around Ω/π = 1.3 and 2.3 are remarkably influenced by the position of the nonlinear interface and oscillate against the frequency due to the finite thickness of the layered structure. Clearly from Eqs. (50) and (51), the reflected and transmitted waves have the identical second-harmonic amplitude when s = N/2, i.e., the nonlinear interface is located exactly at the center of the layered structure.

5.2.2. Spatial distribution of the second-harmonic amplitude inside the multilayered structure

In order to ease the interpretation of the results shown in Fig. 3, the second-harmonic amplitude inside the multilayered structure, given as $U_2(x) \equiv U_{2\mathrm{F}}(x) + U_{2\mathrm{B}}(x) = \mathbf{e}^{\mathrm{T}}\mathbf{U}_2(x)$, is calculated according to the following equations:

$$U_2(x) = \mathbf{e}^{\mathrm{T}}\mathbf{P}\left(2\Omega\frac{x - X_{p-1}}{h}\right)\mathbf{H}(2\Omega)^{p-1}\mathbf{T}_{\mathrm{SL}}\mathbf{U}_2(X_{0-}), \qquad X_{p-1} < x < X_p, \tag{54a}$$

for p = 1, 2, …, s, and

$$U_2(x) = \mathbf{e}^{\mathrm{T}}\mathbf{P}\left(2\Omega\frac{x - X_{p-1}}{h}\right)[\mathbf{H}(2\Omega)^{p-1}\mathbf{T}_{\mathrm{SL}}\mathbf{U}_2(X_{0-}) + \mathbf{b}_s(\Omega)], \qquad X_{p-1} < x < X_p, \tag{54b}$$

for $p = s + 1, s + 2, \ldots, N$.

The spatial distribution of the second-harmonic amplitude corresponding to Fig. 3 is illustrated in Fig. 4, where the positions of the single nonlinear interface and the boundaries between the structure and the semi-infinite media are indicated by arrows and vertical dashed lines, respectively. The imaginary parts of Bloch wavenumber shown in Fig. 2(d) are also depicted at the right in Fig. 4 to compare the frequency dependence of second-harmonic amplitudes with the pass and stop band structure of the corresponding infinitely extended layered structure.

It is seen in Fig. 4 that the generation as well as propagation characteristics of the second-harmonic component in the finite layered structures reflect the band structure of Bloch wave. First, when both fundamental and double frequencies lie in the stop bands of Bloch wave such as at around Ω/π = 0.9, 1.8, and 2.5, the interfacial gap opening $|Y_{1s}(\Omega)|$ becomes small at the leftmost interlayer interface and it further decreases for the rightward nonlinear interfaces as seen in Fig. 2(a) in the case of N = 4. This is because the propagation of the fundamental wave is strongly prohibited. In addition, the generated second-harmonic component is also prohibited from propagating through the multilayered structure as represented by the small value of $|T_1(2\Omega)|$, and such an effect becomes significant for larger N. As a result, both the second-harmonic amplitudes of the reflected and transmitted waves fall to low levels for any positions of the nonlinear interface in these frequency ranges. When s = 1 in Fig. 3, a slight amount of the second-harmonic amplitude can be observed in the reflected wave, since the wave generated at the leftmost nonlinear interface can reach the observation point without being influenced by the layered structure as can be seen in Fig. 4(a), 4(d), and 4(g).

Second, when the fundamental and double frequencies are within one of the pass and stop bands of Bloch wave, respectively, such as at around Ω/π = 0.4, 1.3, and 2.3, the second-harmonic component is generated at any positions of the nonlinear interface, while the generated second-harmonic decays significantly as it propagates in the structure as seen in Fig. 4. Hence, the second-harmonic amplitudes in Fig. 3 remain observable on the left and right sides of the structure only when the leftmost (s = 1) and rightmost ($s = N - 1$) interlayer interfaces possess the nonlinearity, respectively.

Third, in the opposite case of the second one where only the fundamental frequency belongs to one of the stop bands such as at around Ω/π = 1.6, relatively high second-harmonic amplitudes are seen for both reflected and transmitted fields only when s = 1 in Fig. 3. This is because of the larger second-harmonic generation at the leftward nonlinear interfaces compared to the rightward ones and the high propagation efficiency of the second-harmonic component in the structure.

Finally, when the frequency is at around Ω/π = 0.6, Ω/π = 1.1, and Ω/π = 2.05 where both fundamental and double frequencies are within the pass bands, the second-harmonic amplitudes of the reflected and transmitted waves become relatively high regardless of the position of the nonlinear interface due to the unhampered generation as well as propagation efficiency of the second-harmonic component.

5.3. Second-harmonic generation by multiple nonlinear interfaces

When all interlayer interfaces possess the same nonlinearity of $\beta_m = \beta$ (m = 1, 2, …, N–1), the second-harmonic amplitudes on both sides of the multilayered structure are calculated by Eqs. (52) and (53). Their variation with the normalized fundamental frequency is shown in Fig. 5 for N = 4, 10, and 20 with fixed Λ = 0.2 and ζ = 3.

In Fig. 5, the second-harmonic amplitudes of the reflected and transmitted waves exhibit the frequency dependence which combines the features seen above in the case of single nonlinear

interface. In particular, the second-harmonic amplitudes due to the multiple nonlinear interfaces grow almost monotonically with N when the frequency is at around $\Omega/\pi = 1$ and $\Omega/\pi = 2$ in the pass bands of Bloch wave. This is in agreement with the results in Ref. [52] that the second-harmonic generation in infinitely layered structures exhibits a cumulative growth with the number of consecutive nonlinear interfaces at around $\Omega/\pi = k$ ($k = 0, 1, 2, \ldots$), where the phase matching is nearly met for the Bloch waves at the fundamental and double frequencies.

5.4. Influence of non-dimensional parameters on the second-harmonic generation

5.4.1. Relative linear compliance of the interlayer interfaces Λ

In order to examine the influence of the non-dimensional parameter Λ given by Eq. (25) on the second-harmonic generation, the variation of the second-harmonic amplitudes of the 10-layered structure shown in Fig. 5, i.e., $N = 10$, $\zeta = 3$, and $\beta_m = \beta$ ($m = 1, 2, \ldots, N–1$), with Λ is depicted in Fig. 6(a) and 6(b), respectively. The pass and stop bands of Bloch wave in the corresponding infinitely extended layered structure at the fundamental and double frequencies are also shown in Fig. 6(c).

In Fig. 6(c), the frequency ranges in which both fundamental and double frequencies belong to the stop bands become wider as Λ increases from the small value of 10^{-2} where the interlayer interfaces are close to the perfect bonding condition. Such stop band behavior appears clearly in the transmission spectrum in Fig. 6(b). On the other hand, the reflected field in Fig. 6(a) has a relatively high amplitude even when the frequency lies in the white zones in Fig. 6(c). This is because, as discussed above, the second-harmonic component generated at the leftward interlayer interfaces can reach the left side of the multilayered structure even when both fundamental wave and its second-harmonic component are prohibited from propagating in the structure.

5.4.2. Acoustic impedance ratio between the layer and the outside medium ζ

The variation of the second-harmonic amplitude spectra with the non-dimensional parameter ζ

given by Eq. (26) is depicted in Fig. 7 for $N = 10$, $\Lambda = 0.2$, and $\beta_m = \beta$ ($m = 1, 2, \ldots, N-1$). Note that unlike Fig. 6, the band structure of Bloch waves is not shown in Fig. 7 since it is independent of ζ as can be seen from Eqs. (27) and (28). The dispersion relation of Bloch wave corresponding to Fig. 7 is shown in Fig. 2(d).

In Fig. 7, the magnitudes of second-harmonic amplitude in the reflected and transmitted fields are influenced by ζ, while their oscillatory nature against the frequency does not depend on ζ very much. This is because this parameter governs the frequency-independent scattering at the perfect bonding interfaces between the multilayered structure and the surrounding semi-infinite media: the amplitude transmission coefficient of the longitudinal wave across the interface is given by $T_{SL} = 2/(1 + \zeta)$ and $T_{LS} = 2\zeta/(1 + \zeta)$ when the wave impinges from the semi-infinite medium and the layer, respectively.

When ζ becomes large, say, $\zeta = 10^3$, the second-harmonic component is hardly generated at the interlayer interfaces because of the low transmission of incident wave through the interface at $x = X_0$. As a consequence, the second-harmonic amplitudes of the reflected and transmitted waves become vanishingly small except the several sharp peaks caused by the resonance frequencies of the multilayered structure. As ζ decreases therefrom, the second-harmonic generation at the interlayer interfaces becomes larger due to the associated increase of T_{SL}. Further decrease of ζ is, however, accompanied with the decrease of T_{LS}. Therefore, the second-harmonic amplitudes on both sides of the structure increase as ζ goes down from 10^3, while they begin to decrease at around $\zeta = 10^0$ where $T_{SL} = T_{LS} = 1$.

6. Conclusion

The acoustic second-harmonic generation behavior in a multilayered structure with nonlinear spring-type interlayer interfaces has been analyzed theoretically to investigate the frequency

dependence of second-harmonic amplitudes in the reflected and transmitted fields resulting from the normal incidence of a monochromatic longitudinal wave to the structure. Analytical expressions have been derived for the second-harmonic amplitudes of the reflected and transmitted waves by a perturbation analysis combined with the transfer-matrix method. The frequency dependence of the second-harmonic amplitudes due to a single nonlinear interface has been shown to reflect the band structure of the Bloch wave for the corresponding infinitely extended layered structure and to depend remarkably on the position of the nonlinear interface as well as the number of layers. When all interlayer interfaces possess the identical nonlinearity, the second-harmonic amplitudes on both sides of the structure have been found to increase almost monotonically with the number of layers in the frequency ranges where both fundamental and double frequencies lie in the pass bands of Bloch wave. The bandwidth of the frequency ranges in which the second-harmonic amplitude drops to relatively low levels has been shown to be profoundly influenced by the relative linear compliance of the interlayer interfaces, while the acoustic impedance ratio between the layer and the surrounding medium has been shown to have an effect to mainly vary the magnitude of second-harmonic amplitudes. The results obtained in the present analysis can be helpful when characterizing the imperfect interlayer interfaces of multilayered structures by using nonlinear acoustic methods.

Acknowledgments

This work has been supported by JSPS KAKENHI Grant Numbers JP16H06871 and JP15K13833.

References

[1] K. Kendall, D. Tabor, An ultrasonic study of the area of contact between stationary and sliding surfaces, Proc. R. Soc. Lond. A323 (1971) 321-340.

[2] J.-M. Baik, R. B. Thompson, Ultrasonic scattering from imperfect interfaces: a quasi-static model, J. Nondestruct. Eval. 4 (1984) 177-196.

[3] A. Boström, G. Wickham, On the boundary conditions for ultrasonic transmission by partially closed cracks, J. Nondestruct. Eval. 10 (1991) 139-149.

[4] S. I. Rokhlin, Y. J. Wang, Analysis of boundary conditions for elastic wave interaction with an interface between two solids, J. Acoust. Soc. Am. 89 (1991) 503-515.

[5] P. B. Nagy, Ultrasonic classification of imperfect interfaces, J. Nondestruct. Eval. 11 (1992) 127-139.

[6] S. I. Rokhlin, Y. J. Wang, Equivalent boundary conditions for thin orthotropic layer between two solids: Reflection, refraction, and interface waves, J. Acoust. Soc. Am. 91 (1992) 1875-1887.

[7] S. I. Rokhlin, W. Huang, Ultrasonic wave interaction with a thin anisotropic layer between two anisotropic solids: Exact and asymptotic-boundary condition methods, J. Acoust. Soc. Am. 92 (1992) 1729-1742.

[8] B. W. Drinkwater, R. S. Dwyer-Joyce, P. Cawley, A study of the interaction between ultrasound and a partially contacting solid-solid interface, Proc. R. Soc. Lond. A452 (1996) 2613-2628.

[9] A. M. Quinn, B. W. Drinkwater, R. S. Dwyer-Joyce, The measurement of contact pressure in machine elements using ultrasound, Ultrasonics 39 (2002) 495-502.

[10] R. S. Dwyer-Joyce, The application of ultrasonic NDT techniques in tribology, Proc. IMechE Part J: Eng. Trib., 219 (2005), pp. 347-366.

[11] S. Biwa, S. Hiraiwa, E. Matsumoto, Stiffness evaluation of contacting surfaces by bulk and interface waves, Ultrasonics 47 (2007) 123-129.

[12] N. Mori, S. Biwa, T. Hayashi, Reflection and transmission of Lamb waves at an imperfect joint of plates, J. Appl. Phys. **113** (2013) 074901.

[13] N. Mori, S. Biwa, Resonance of an imperfect joint of plates by the lowest-order symmetric Lamb mode, J. Acoust. Soc. Am. **137** (2015) 3139-3148.

[14] C. Pecorari, Scattering of a Rayleigh wave by a surface-breaking crack with faces in partial contact, Wave Motion 33 (2001) 259-270.

[15] A. M. Lomonosov, P. V. Grigoriev, P. Hess, Sizing of partially closed surface-breaking microcracks with broadband Rayleigh waves, J. Appl. Phys. 105 (2009) 084906.

[16] M. V. Golub, Propagation of elastic waves in layered composites with microdefect concentration zones and their simulation with spring boundary conditions, Acoust. Phys. 56 (2010) 848-855.

[17] M. V. Golub, A. Boström, Interface damage modeled by spring boundary conditions for in-plane elastic waves, Wave Motion 48 (2011) 105-115.

[18] M. V. Golub, O. V. Doroshenko, A. Boström, Effective spring boundary conditions for a damaged interface between dissimilar media in three-dimensional case, Int. J. Solids Struct. 81 (2016) 141-150.

[19] L. J. Pyrak-Nolte, N. G. W. Cook, Elastic interface waves along a fracture, Geophys. Res. Lett. 14 (1987) 1107-1110.

[20] L. J. Pyrak-Nolte, L. R. Myer, N. G. W. Cook, Transmission of seismic waves across single natural fractures, J. Geophys. Res. 95 (1990) 8617-8638.

[21] B. Gu, K. T. Nihei, L. R. Myer, L. J. Pyrak-Nolte, Fracture interface waves, J. Geophys. Res. 101 (1996) 827-835.

[22] L. J. Pyrak-Nolte, The seismic response of fractures and the interrelations among fracture properties, Int. J. Rock Mech. Min. Sci. & Geomech. Abstr. 33 (1996) 787-802.

[23] B. Gu, R. Suáres-Rivera, K. T. Nihei, L. R. Myer, Incidence of plane waves upon a fracture, J. Geophys. Res. 101 (1996) 25,337-25,346.

[24] A. I. Lavrentyev, S. I. Rokhlin, Ultrasonic spectroscopy of imperfect contact interfaces between a layer and two solids, J. Acoust. Soc. Am. **103** (1998) 657-664.

[25] A. Baltazar, L. Wang, B. Xie, S. I. Rokhlin, Inverse ultrasonic determination of imperfect interfaces and bulk properties of a layer between two solids, J. Acoust. Soc. Am. **114** (2003) 1424-1434.

[26] B. Hosten, M. Castaings, Finite elements methods for modeling the guided waves propagation in structures with weak interfaces, J. Acoust. Soc. Am. **117** (2005) 1108-1113.

[27] B. L. Crom, M. Castaings, Shear horizontal guided wave modes to infer the shear stiffness of adhesive bond layers, J. Acoust. Soc. Am. **127** (2010) 2220-2230.

[28] M. Castaings, SH ultrasonic guided waves for the evaluation of interfacial adhesion, Ultrasonics 54 (2014) 1760-1775.

[29] Y. Lu, J. D. Achenbach, Effects of random deviations in interface properties on the propagation of ultrasound in thick composites, J. Acoust. Soc. Am. 90 (1991) 2576-2585.

[30] Y. Lu, Effects of random fluctuations in ply mechanical properties on ultrasound propagation in a laminated solid layer, Ultrasonics 30 (1992) 289-295.

[31] Y. Ishii, S. Biwa, Ultrasonic evaluation of interlayer interfacial stiffness of multilayered structures, J. Appl. Phys. 111 (2012) 084907.

[32] Y. Ishii, S. Biwa, Evaluation of interlayer interfacial stiffness and layer wave velocity of multilayered structures by ultrasonic spectroscopy, J. Acoust. Soc. Am. 136 (2014) 183-191.

[33] Y. Ishii, S. Biwa, Transmission of ultrasonic waves at oblique incidence to composite laminates with spring-type interlayer interfaces, J. Acoust. Soc. Am. 138 (2015) 2800-2810.

[34] J. B. Zhu, X. B. Zhao, J. C. Li, G. F. Zhao, J. Zhao, Normally incident wave propagation across a joint set with the virtual wave source method, J. Appl. Geophys. 73 (2011) 283-288.

[35] J. B. Zhu, J. Zhao, Obliquely incident wave propagation across rock joints with virtual wave

source method, J. Appl. Geophys. 88 (2013) 23-30.
[36] O. Buck, W. L. Morris, J. M. Richardson, Acoustic harmonic generation at unbonded interfaces and fatigue cracks, Appl. Phys. Lett. 33 (1978) 371-373.
[37] J. M. Richardson, Harmonic generation at an unbonded interface, I. Planar interface between semi-infinite elastic media, Int. J. Engng Sci. 17 (1979) 73-85.
[38] A. M. Sutin, V. E. Nazarov, Nonlinear acoustic methods of crack diagnosis, Radiophys. Quant. Electr. 38 (1995) 109-120.
[39] I. Y. Solodov, Ultrasonics of non-linear contacts: propagation, reflection and NDE-applications, Ultrasonics 36 (1998) 383-390.
[40] C. J. Brotherhood, B. W. Drinkwater, S. Dixon, The detectability of kissing bonds in adhesive joints using ultrasonic techniques, Ultrasonics 41 (2003) 521-529.
[41] J. –P. Jiao, W. –H. Liu, C. –F. He, B. Wu, J. Zhang, Nonlinear acoustic interaction of contact interfaces, Exp. Mech. 54 (2014) 63-68.
[42] C. Pecorari, Nonlinear interaction of plane ultrasonic waves with an interface between rough surfaces in contact, J. Acoust. Soc. Am. 113 (2003) 3065–3072.
[43] S. Biwa, S. Nakajima, N. Ohno, On the acoustic nonlinearity of solid-solid contact with pressure-dependent interface stiffness, Trans. ASME J. Appl. Mech. 71 (2004) 508-515.
[44] C. Pecorari, M. Poznic, On the linear and nonlinear acoustic properties of dry and water-confining elasto-plastic interfaces, Proc. R. Soc. A462 (2006) 769-788.
[45] S. Biwa, S. Hiraiwa, E. Matsumoto, Experimental and theoretical study of harmonic generation at contacting interface, Ultrasonics 44 (2006) e1319-e1322.
[46] J.–Y. Kim, A. Baltazar, J. W. Hu, S. I. Rokhlin, Hysteretic linear and nonlinear acoustic responses from pressed interfaces, Int. J. Solids Struct. 43 (2006) 6436-6452.
[47] J. –Y. Kim, J. –S. Lee, A micromechanical model for nonlinear acoustic properties of interfaces between solids, J. Appl. Phys. 101 (2007) 043501.
[48] T. Nam, T. Lee, C. Kim, K. –Y. Jhang, N. Kim, Harmonic generation of an oblique incident ultrasonic wave in solid-solid contact interfaces, Ultrasonics 52 (2012) 778-783.
[49] D. Yan, B. W. Drinkwater, S. A. Neild, Measurement of the ultrasonic nonlinearity of kissing bonds in adhesive joints, NDT&E Int. 42 (2009) 459-466.
[50] D. Yan, S. A. Neild, B. W. Drinkwater, Modelling and measurement of the nonlinear behavior of kissing bonds in adhesive joints, NDT&E Int. 47 (2012) 18-25.
[51] S. Junca, B. Lombard, Interaction between periodic elastic wave and two contact nonlinearities, Math. Models Methods Appl. Sci. 22 (2012) 1150022.
[52] S. Biwa, Y. Ishii, Second-harmonic generation in an infinite layered structure with nonlinear spring-type interfaces, Wave Motion 63 (2016) 55-67.
[53] Y. Ishii, S. Biwa, Acoustic harmonic generation in a multilayered structure with nonlinear interfaces, Nonlinear Acoustics, State-of-the-Art and Perspectives: 19th International Symposium

on Nonlinear Acoustics (eds. T. Kamakura and N. Sugimoto); AIP Conference Proceedings 1474 (2012) 223-226.

[54] T. Thomson, Transmission of elastic waves through a stratified solid medium, J. Appl. Phys. 21 (1950) 89-93.

[55] N. A. Haskell, The dispersion of surface waves on multilayered media, Bull. Seismol. Soc. Am. 43 (1953) 17-34.

[56] J. M. Bendickson, J. P. Dowling, M. Scalora, Analytic expressions for the electromagnetic mode density in finite, one-dimensional, photonic band-gap structures, Phys. Rev. E 53 (1996) 4117-4121.

Figure captions

Fig. 1 A multilayered structure consisting of N linear elastic layers and N-1 spring-type interlayer interfaces embedded between two linear elastic semi-infinite media.

Fig. 2 Frequency dependence of (a) the interfacial gap opening, (b) the amplitude transmission coefficient of fundamental wave, (c) the factor $|E_s(\Omega)|$, (d) the dispersion relation of forward-propagating Bloch wave in the corresponding infinitely extended layered structure, and (e) the factor $|E_s(2\Omega)|$ when $N = 4$, $\Lambda = 0.2$, and $\zeta = 3$.

Fig. 3 Frequency dependence of the second-harmonic amplitudes of the reflected and transmitted waves due to a single nonlinear interface located at $x = X_1$, $x = X_{N/2}$, and $x = X_{N-1}$ when (a) and (b) $N = 4$, (c) and (d) $N = 10$, and (e) and (f) $N = 20$, for $\Lambda = 0.2$ and $\zeta = 3$.

Fig. 4 Spatial distrtibution of the second-harmonic amplitude of Fig. 3. The arrows and vertical dashed lines represent the positions of nonlinear interface and both ends of the multilayered structure, respectively. The imaginary parts of Bloch wavenumber in Fig. 2(d) are also shown at the right.

Fig. 5 Frequency dependence of the second-harmonic amplitudes of the (a) reflected and (b) transmitted waves due to multiple nonlinear interfaces when $N = 4$, 10, and 20, for $\Lambda = 0.2$ and $\zeta = 3$.

Fig. 6 Variation of the frequency dependence of second-harmonic amplitudes of the (a) reflected and (b) transmitted waves due to multiple nonlinear interfaces with Λ when $N = 10$ and $\zeta = 3$. (c) Band structures of Bloch wave in the corresponding infinitely extended layered structures at the fundamental and double frequencies.

Fig. 7 Variation of the frequency dependence of second-harmonic amplitudes of the (a) reflected and (b) transmitted waves due to multiple nonlinear interfaces with ζ when $N = 10$ and $\Lambda = 0.2$.

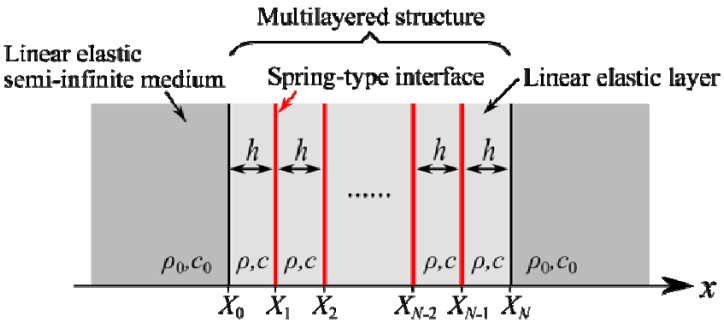
Multilayered structure
Linear elastic
semi-infinite medium
Spring-type interface
Linear elastic layer
h
h
h
h
.....
ρ0,c0
ρ,c
ρ,c
ρ,c
ρ,c
ρ0,c0
x
X0
X1
X2
XN-2
XN-1
XN

Fig. 1

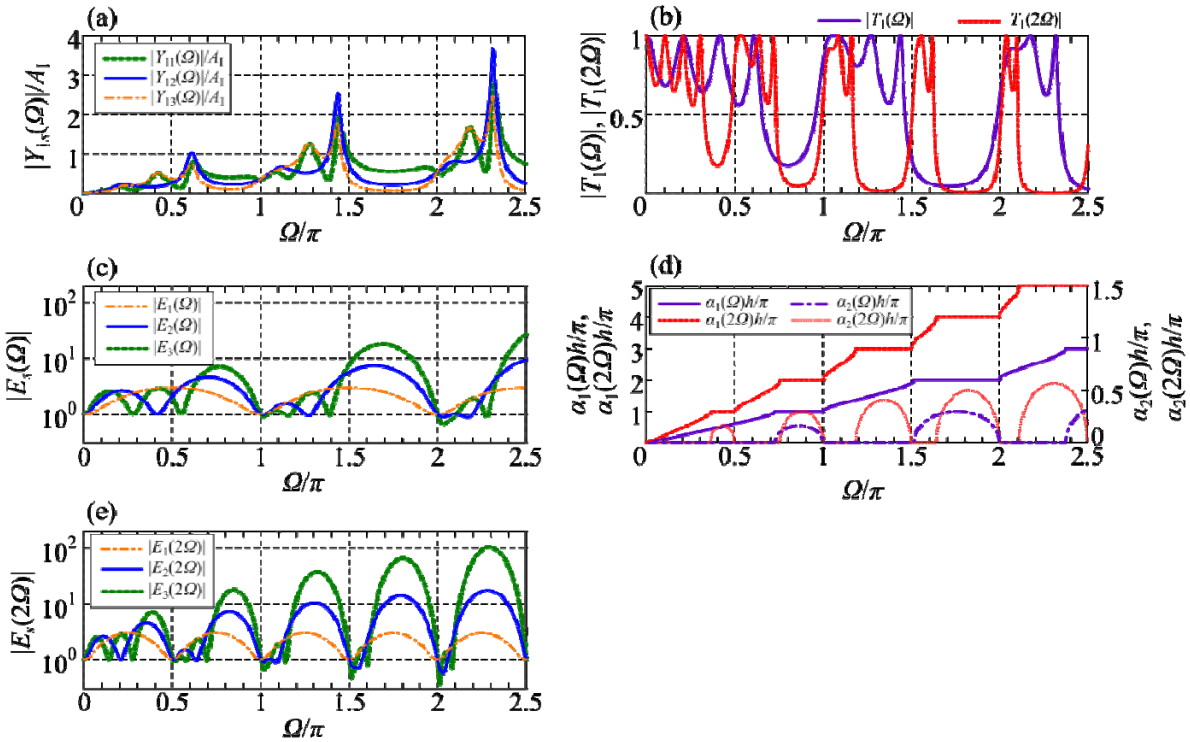
(a)
(b)
(c)
(d)
(e)
Ω/π

Fig. 2

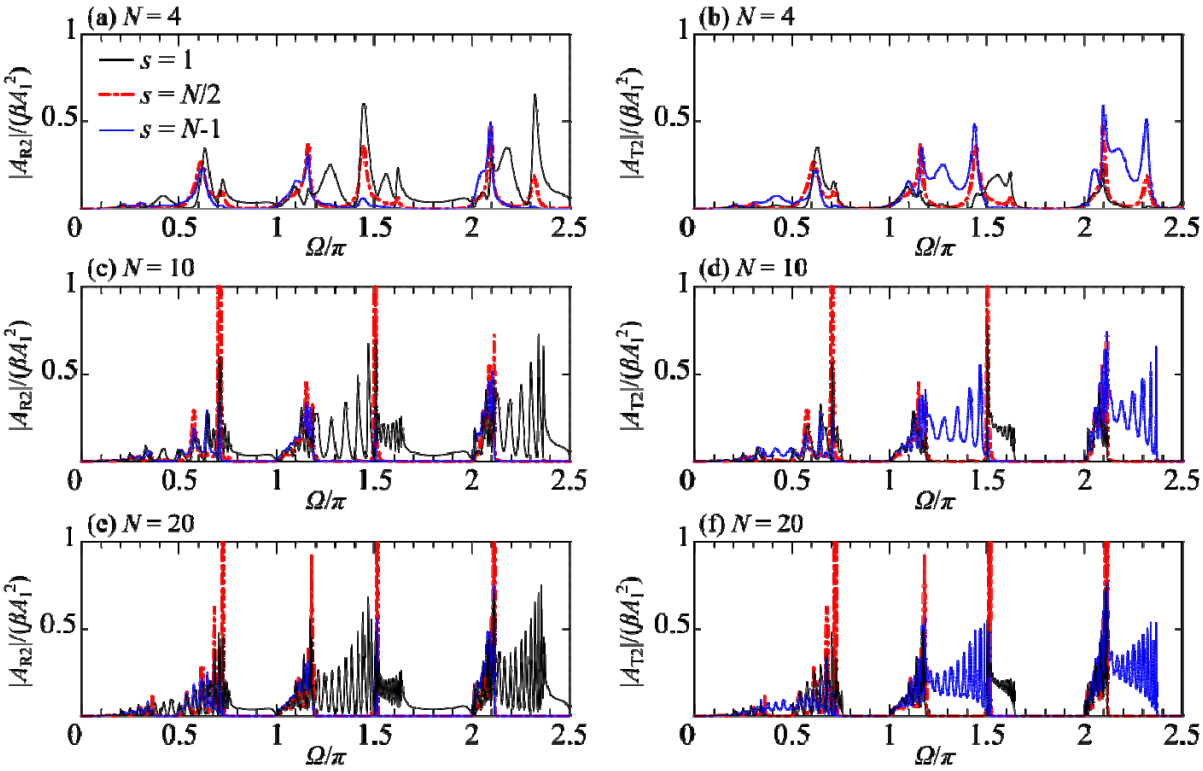
(a) N = 4
(b) N = 4
(c) N = 10
(d) N = 10
(e) N = 20
(f) N = 20
s = 1
s = N/2
s = N-1
|A_R2|/(βA_I^2)
|A_T2|/(βA_I^2)
Ω/π
0
0.5
1
1.5
2
2.5

Fig. 3

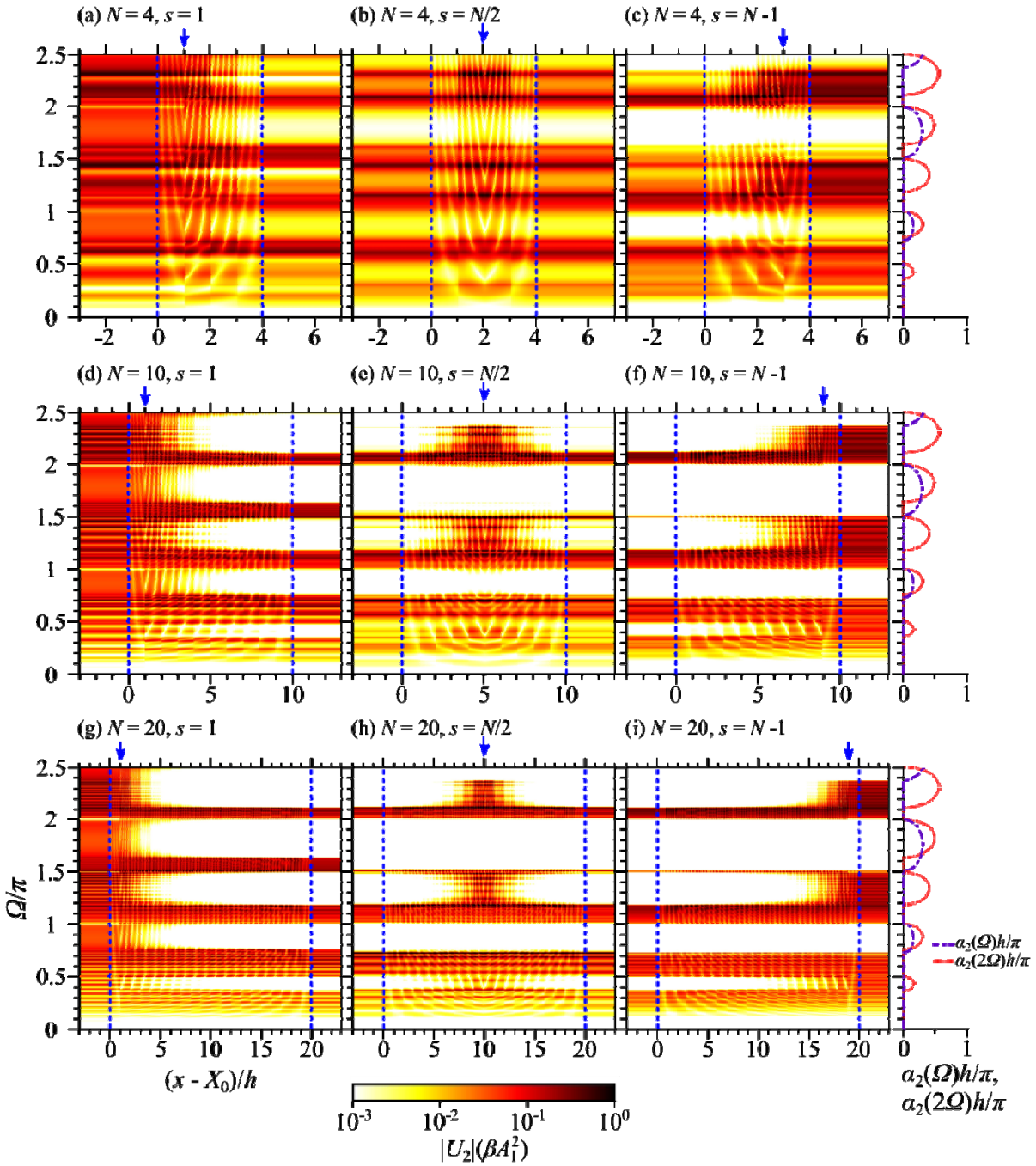
(a) N = 4, s = 1
(b) N = 4, s = N/2
(c) N = 4, s = N -1
(d) N = 10, s = 1
(e) N = 10, s = N/2
(f) N = 10, s = N -1
(g) N = 20, s = 1
(h) N = 20, s = N/2
(i) N = 20, s = N -1
Ω/π
(x - X0)/h
α2(Ω)h/π
α2(2Ω)h/π
α2(Ω)h/π,
α2(2Ω)h/π
|U2|(βA1^2)

Fig. 4

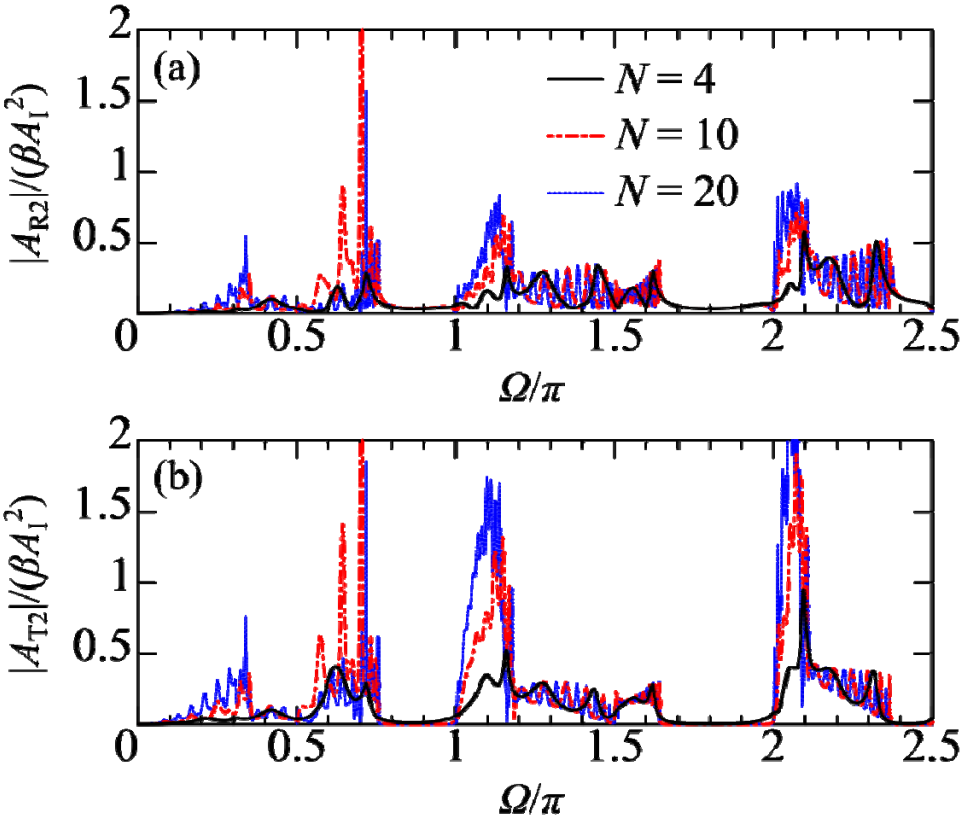
(a)
(b)
N = 4
N = 10
N = 20
|A_R2|/(βA_I^2)
|A_T2|/(βA_I^2)
Ω/π
0
0.5
1
1.5
2
2.5

Fig. 5

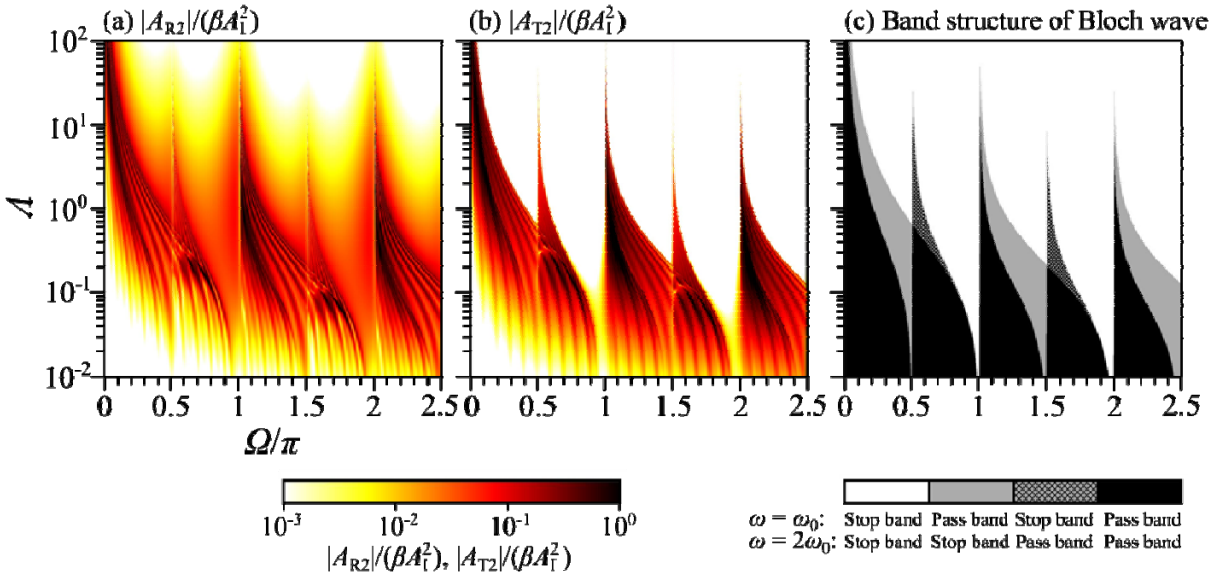
(a) |A_R2|/(βA_I^2)
(b) |A_T2|/(βA_I^2)
(c) Band structure of Bloch wave
Λ
Ω/π
10^2
10^1
10^0
10^-1
10^-2
0
0.5
1
1.5
2
2.5
10^-3
10^-2
10^-1
10^0
|A_R2|/(βA_I^2), |A_T2|/(βA_I^2)
ω = ω0: Stop band Pass band Stop band Pass band
ω = 2ω0: Stop band Stop band Pass band Pass band

Fig. 6

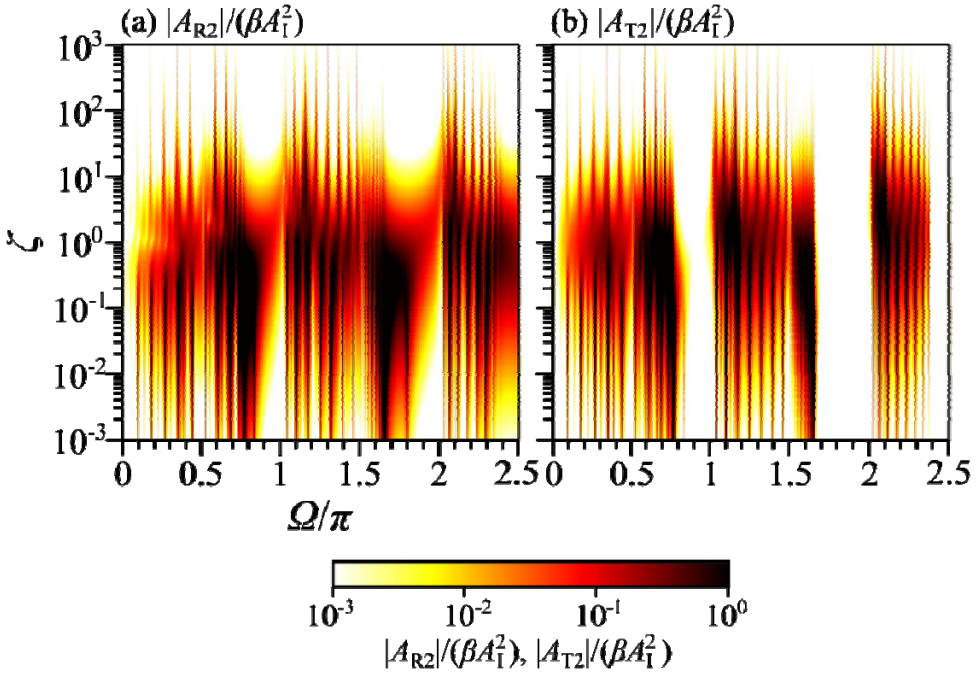
(a) $|A_{R2}|/(\beta A_I^2)$
(b) $|A_{T2}|/(\beta A_I^2)$
10^3
10^2
10^1
10^0
10^{-1}
10^{-2}
10^{-3}
ζ
0
0.5
1
1.5
2
2.5
Ω/π
10^{-3}
10^{-2}
10^{-1}
10^0
$|A_{R2}|/(\beta A_I^2)$, $|A_{T2}|/(\beta A_I^2)$

Fig. 7